Air nanobubbles retard calcite crystal growth

Tagomori, Ken
Department of Earth Resources Engineering, Kyushu University

Kioka, Arata
Department of Earth Resources Engineering, Kyushu University

Nakagawa, Masami
Department of Mining Engineering, Colorado School of Mines

Ueda, Akira
Department of Environmental Biology and Chemistry, University of Toyama

他

出版情報：Colloids and Surfaces A: Physicochemical and Engineering Aspects. 648, pp.129319-, 2022-09-05. Elsevier
バージョン：
権利関係：

Air nanobubbles retard calcite crystal growth

Ken Tagomori (1), **Arata Kioka** (1,*), **Masami Nakagawa** (2), **Akira Ueda** (3), **Kenji Sato** (4), **Kotaro Yonezu** (1), **Satoshi Anzai** (5)

1. Department of Earth Resources Engineering, Kyushu University, Fukuoka, Japan
2. Department of Mining Engineering, Colorado School of Mines, Golden, CO, USA
3. Department of Environmental Biology and Chemistry, University of Toyama, Toyama, Japan
4. Technology Department, Furusato Geothermal Power Corp., Oguni, Kumamoto, Japan
5. Anzaikantetsu Co. Ltd., Yokohama, Japan

*Corresponding author:
kioka@mine.kyushu-u.ac.jp; +81-92-802-3343 (A. Kioka)
Department of Earth Resources Engineering, Faculty of Engineering, Kyushu University, Nishi-ku, Fukuoka 819-0395, Japan.

Abstract (219 words)

Demands for "green" additives that control the crystal growth and inhibit the scale formation in industrial processes are growing as never before. Nanobubbles can be the green additive for inhibiting and/or promoting the crystal growth of calcium carbonate, given their well-known unique physicochemical properties. This paper reports for the first time the changes in the crystal growth rate of calcite in liquid in the presence of air nanobubbles. We injected the air nanobubbles into the solution and studied the calcite crystal growth for the first 4 hours in a static condition at 20°C and 88°C. We found that air nanobubbles retarded the growth rate of calcite crystal by up to 53% and 33% at 20°C and 88°C, respectively. The retardation of calcite crystal growth could differ with different number densities of air nanobubbles added to the solution. A higher number density of nanobubbles generally showed slightly greater retardation throughout the tested 4 hours. Air nanobubbles may influence the crystal growth either by changing solid-liquid interfacial tension on the crystal surface, reducing the free growth sites, adsorbing Ca^{2+} ions, playing roles in bubble mattress and thermal buffering on the crystal surface, or combinations of them. Our findings suggest that air nanobubbles can be utilized as a green inhibitor of calcite crystal growth and calcium carbonate scale in broad industrial areas.

Keywords
Crystal growth; Nanobubbles; Calcium carbonate; Calcite; Green inhibitor; Scale formation

Published in *Colloids and Surfaces A: Physicochemical and Engineering Aspects*
Received 3 April 2022, Revised 10 May 2022, Accepted 24 May 2022.
https://doi.org/10.1016/j.colsurfa.2022.129319

Graphical Abstract

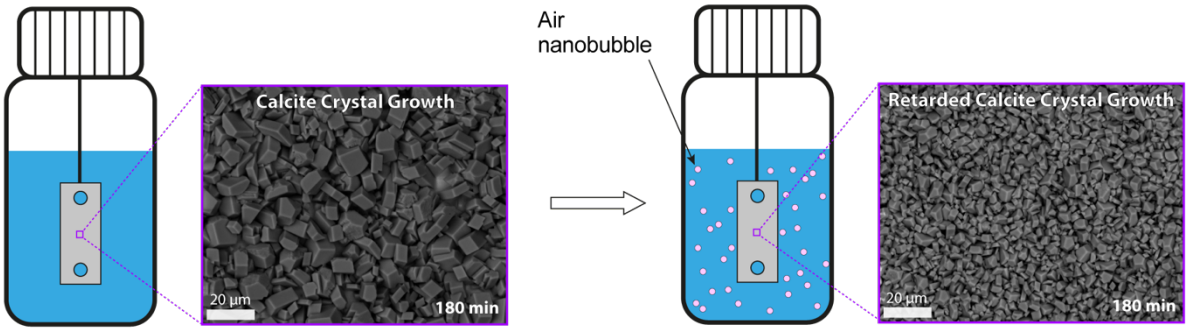

Calcite crystal growth was retarded in the presence of air nanobubbles at 20°C and 88°C.

Highlights (3 to 5 bullet points, max. 85 characters each)

- Calcite crystal growth was retarded by adding air nanobubbles at 20°C and 88°C
- The retardation efficiencies of crystal growth were up to 53% (20°C) and 33% (88°C)
- Nanobubbles influence the crystal-liquid interface and the substrate surface
- Air nanobubbles can be a "green" and inexpensive inhibitor for $CaCO_3$ crystal growth

1. Introduction

Crystallization draws interest from the broad discipline that spans scale formation, corrosion and abrasion, frost heave, biomineralization, protein structure analyses, pharmaceuticals, and the synthesis of nanomaterials. The crystallization processes are determined by the nucleation and the rate of growth. Numerous efforts are thus made to understand their mechanisms and develop strategies to efficiently control the size and shape of crystals [1,2]. As for promoting crystal growth, many inorganic and organic materials have been studied historically due to intensive pharmaceutical interests. In contrast, the additives to inhibit crystal growth are less studied and generally categorized into low molecular weight phosphonates, polymeric carboxylates such as polyacrylates, and polymer polyvinylpyrrolidone [3 – 5]. Among our interests in a broad discipline of crystal growth, calcium carbonate, comprising more than 4% of the Earth's crust, plays a significant role in the long-term global CO_2 cycle [6]. Understanding of geological, climate, biomineralization and industrial processes involving the calcium carbonate system attributes to the knowledge regarding mechanisms and rates of calcium carbonate crystal growth [7]. Amorphous calcium carbonate (ACC) is thermodynamically unstable and transforms rapidly to calcite, vaterite, or aragonite unless it is kinetically stabilized [8 – 10]. Calcite is rhombohedral and among the most stable polymorph of calcium carbonate. Although calcite is a simple compound, its growth rate varies considerably with many factors such as temperature, pH, saturation index and the Ca^{2+} to CO_3^{2-} ratio [11,12]. Soluble chemical additives are now more often used to produce crystals with the desired morphologies, sizes, and structures. These inhibitors adsorb to growing calcite crystals and bind to the growth sites, which results in inhibiting the crystal growth and/or unsettling the regular crystal shape leading to the weakening of crystal stability [13,14]. Yet, the detailed effects and various mechanisms of additives on the growth and morphological changes of calcite crystals are still not well understood, hampering to improve to control them. Moreover, there are growing demands for environmental-friendly and inexpensive "green" additives that can control crystal growth, compared with the chemical products commonly used.

Nanobubbles with a typical diameter of 50–200 nm can exist in liquids and at the solid-liquid interface, and they have unique physicochemical properties [15]. In contrast to microbubbles, the most peculiar characteristic of bulk nanobubbles is their longevity. Many works [16 – 18] have reported that nanobubbles can stably remain in liquid for weeks and months rather than microseconds theoretically argued. Nanobubbles favor being pinned and staying for a long time on a rough surface. The surface nanobubbles have also been recognized to pose a profound impact on the solid-liquid interaction by changing the two-phase contact to a three-phase contact [19 – 21]. Also, nanobubbles are stable with respect to an increase in temperature [22,23], and their stability is generally not sensitive to the pH of aqueous solution [24]. Thus, nanobubbles influence the surface condition through hydrodynamic controlling of the solid-liquid interface, allowing a broad range of applications. The high surface area and interfacial free energy of nanobubbles could replace or augment the current fouling mitigation strategies [25 – 27]. The use of nanobubbles is expected to benefit in preventing chemical pollution and reducing the cost of inhibiting scale formation of calcium carbonate, compared with the chemical products commonly used.

An earlier work [28] provided a theoretical perspective on the effectiveness of nanobubbles for inhibiting the scale formation of calcium carbonate. However, no previous studies have investigated whether nanobubbles can be an inhibitor or promoter for the

crystal growth of any inorganic particles. To the best of our knowledge, this is the first paper that studies whether nanobubbles inhibit or promote the crystal growth of calcite by batch experiments. Our experiment uses the nanobubbles generated by air because the use of air for generating nanobubbles is most practical in any industrial use when they can be either an inhibitor or promoter of the crystal growth. Kim et al. [29] revealed that additives do not affect the morphology of calcite crystals until the crystals reach certain sizes of 0.1–1 μm. We thus study how air nanobubbles influence the calcite crystal growth for the first couple of hours, where the size of calcite crystal changes from ~1 μm to ~10 μm.

2. Materials and methods

2.1. Material and Experiment

We generated air nanobubbles and injected them into ultrapure water (PURELAB Flex 3, ELGA, UK) using an ultrafine-pore ceramic rotational-column nanobubble generator (Anzaikantetsu Co. Ltd., Yokohama, Japan; Figure 1). The number density of generated nanobubbles (nanobubble concentration) increases with the generation time when the rotational speed of the generator's ceramic column is constant [28]. We prepared the air-nanobubbles containing pure water with different levels of bubble number density by changing the time of continuous nanobubble generation at a constant rotational speed of 1,000 rpm: low-number density (generated continuously for 2 min), moderate-number density (5 min) and high-number density (30 min). Air nanobubbles were generated in a 3-liter container at the temperature of 20°C with an injection pressure of 0.05 MPa using an air compressor. The number density of the nanobubbles generated by the studied device is at least on the order of magnitude of 10^8 bubbles per mL, and it generally increases linearly with the generation time at the constant injection pressure and rotational speed. The typical diameter of generated nanobubbles depends on the pore size of the ceramic membrane and injected gas pressure [30], and their mean diameter is 80–90 nm at the injection pressure in our nanobubble generator [28].

We prepared 1 L of the solution with adding air nanobubbles as follows: (1) we dissolved 12.54 g of Sodium hydrogen carbonate ($NaHCO_3$; FUJIFILM Wako Pure Chemical Corporation, Japan) in 500 mL of ultrapure water (30 mM/L), (2) dissolved 22.04 g of Calcium chloride dihydrate ($CaCl_2{\cdot}2H_2O$; FUJIFILM Wako Pure Chemical Corporation, Japan) very gently in 500 mL of the air-nanobubbles-containing pure water (30 mM/L) and (3) mixed the $NaHCO_3$ solution and the $CaCl_2{\cdot}2H_2O$ + air-nanobubbles solution. Likewise, we prepared 1 L of untreated solution as the reference solution by mixing equivalent volumes of 30 mM/L of $NaHCO_3$ and 30 mM/L of $CaCl_2{\cdot}2H_2O$. We then transferred the reference and the air-nanobubbles-containing solutions to pre-cleaned polypropylene bottles (SCC iBoy, 250 mL; AS ONE Corporation, Japan). The bottles have caps to prevent any gas leakage (Figure 1). The studied substrate material for crystal growth of calcium carbonate was the austenitic stainless steel "SUS304" (JIS G4303 Standards) equivalent to the 18/8 stainless steel (UNS S30400/EN 1.4305) with the following chemical composition (wt%): C ≤ 0.08, Si ≤ 1.00, Mn ≤ 2.00, P ≤ 0.045, S ≤ 0.030, 8.0 ≤ Ni ≤ 10.50, 18.0 ≤ Cr ≤ 20.0 and the rest is Fe. The substrate had a dimension of 20×50×1.0 mm (width×length×thickness) and the two holes with 6.5-mm diameters that were used to suspend the substrate in the tested solution using a PTFE string. The stainless substrates were immersed in the bottles of the reference

solution and the air-nanobubbles containing solution for 0.5, 1.0, 2.0, 3.0, and 4.0 hours (Figure 1). An external mechanical disturbance was minimized throughout the experiment. The pH generally decreased with time from ~6.2 (0.5 h) to ~5.9 (4.0 h) and did not show a significant difference between the reference solution and the air-nanobubbles-containing solution throughout this experiment.

To examine the influence of temperature on how nanobubbles react with calcium carbonate particles, we experimented with two different temperatures: (i) the temperature of 20°C and (ii) the elevated temperature of 88°C. Nanobubbles are known to exist at least up to 95°C in water because they can pin a micro-droplet from the receding water over the surface [22]. We thus selected the temperature of 88°C as the experiment for the high-temperature condition (ii), well below the known upper limit of temperature for the presence of nanobubbles. The temperature was kept constant at 88.0±1.0°C by using a water bath. The saturation indices of calcite for the solutions at 20°C and 88°C, determined using RHREEQC version 3 [31] with the database [32], were respectively 0.34 and 1.10 at the beginning of the experiment.

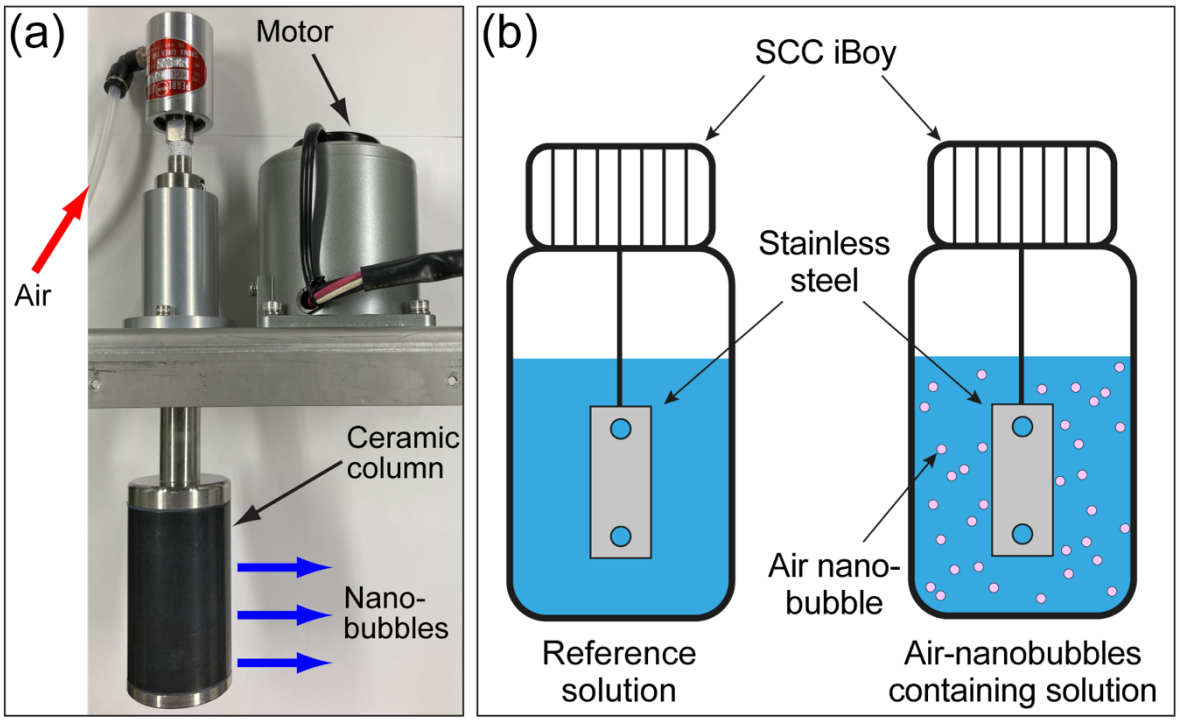

Figure 1: (a) Ultrafine-pore ceramic rotational-column nanobubble generator (Anzaikantetsu Co. Ltd., Yokohama, Japan). Modified from Ref. [28]. (b) Schematic illustrations of immersion test in this study.

2.2. Analyses

The substrates were taken out of the reference and the air-nanobubbles containing solutions in the polypropylene bottles after immersions for 0.5, 1.0, 2.0, 3.0, and 4.0 h to observe changes in the crystal growth and deposition of calcium carbonate at the respective time. After carefully cleaning the substrates using pure water and drying them, we imaged the magnitude of crystal growth of calcium carbonate on the substrate at the respective time by Scanning Electron Microscope (SEM) using a HITACHI SU3500 at the Center of

Advanced Instrumental Analysis, Kyushu University. We obtained SEM images with low and high magnifications (×50 and ×1000). Using the high magnification (×1000) SEM images, we investigated the difference between crystal growth in the reference and air-nanobubbles-containing solutions. We used a method of image analysis for SEM images [33] to compute the crystal sizes, after segmenting crystals and their backgrounds using Otsu's multi-level thresholding [34] with 16 levels of quantization. We obtained the mean diameter and one standard deviation (Mean±1STD) of the crystals in the reference and air-nanobubbles-containing solutions at the respective time by computing the number of pixels of the detected planes of segmented crystals. In addition to quantifying the crystal sizes, we estimated the change in thickness of calcium carbonate deposition on the substrate to quantify the effect in the presence of nanobubbles. The volume-averaged thickness of deposition $h(t)$ (μm) at the respective time t (h) was calculated by:

$$h(t) = \frac{m(t)\times 10^4}{A(t)\times \rho}, \quad (1)$$

where $m(t)$ is the amount of deposited calcium carbonate (g) at the respective time t (h), $A(t)$ is the area of the substrate covered by calcium carbonate (cm^2) at the respective time t (h) and ρ is the density of calcite (g/cm^3). The amount of deposited calcium carbonate can simply be calculated by weighing the substrates before and after immersion for the respective time, because the corrosion suffered in the studied austenitic stainless-steel substrates at the studied pH is negligible. In our experiment, we did not weigh the substrates immersed for 4.0 h because we confirmed many calcium carbonate particles fell off the substrates in the reference solution. The area of the substrate covered by calcium carbonate at the respective time $A(t)$ was estimated using low magnification (×50) SEM images by the conventional threshold algorithm [35] available in the ImageJ/Fiji software [36,37].

3. Results and discussion

3.1. Results at 20°C

We observed the crystal growth of calcium carbonate on the substrate surfaces for the first 4 hours immersed in the reference and the air-nanobubbles-containing solutions. We generated the air-nanobubbles containing solution with different bubble number densities by changing the time of continuous nanobubble generation: low-number density (continuous generation for 2 min), moderate-number density (5 min) and high-number density (30 min) kept at 20.0°C. Immersed substrates were sampled from the reference solution and the air-nanobubbles containing solution after 0.5, 1.0, 2.0, 3.0, and 4.0 h.

The weight change of calcite deposited on the substrate surface $m(t)$ increased gradually through time, from 14.9 mg (0.5 h) to 29.2 mg (3.0 h) for the reference solution. However, we found that the deposited amounts of calcite in the air-nanobubbles-containing solution were lower than those in the reference solution (Figure 2a). For example, the weight changes in the air-nanobubbles containing solutions with moderate-number densities after 0.5 and 1.0 h were 5.2 mg and 8.1 mg, respectively, indicating that air nanobubbles helped inhibit approximately 70% of calcite deposition in the first 1.0 h. Also, areal extents of calcite deposition on the substrate surface $A(t)$ increased gradually with time, from 74.3% (0.5 h) to 92.2% (3.0 h). The areal extents in the air-nanobubbles containing solution with any bubble number densities were lower than those in the

reference solution (Figure 2b). The resulting averaged thickness of calcite deposition on the substrate surfaces $h(t)$ in the air-nanobubbles containing solution with moderate- and high-number densities was well less than that in the reference solution (Figure 2c), demonstrating that air nanobubbles inhibited up to 39% in thickness as compared with the reference solution. On the other hand, the results with a low number density of air nanobubbles were quite similar to those in the reference solution after 1.0, 2.0, and 3.0 h, although we found a significant reduction in the areal extent (50%) with the low-number air-nanobubbles containing solution for the first 0.5 h. These results suggest that air nanobubbles with a bubble number density above a certain value can inhibit calcite deposition.

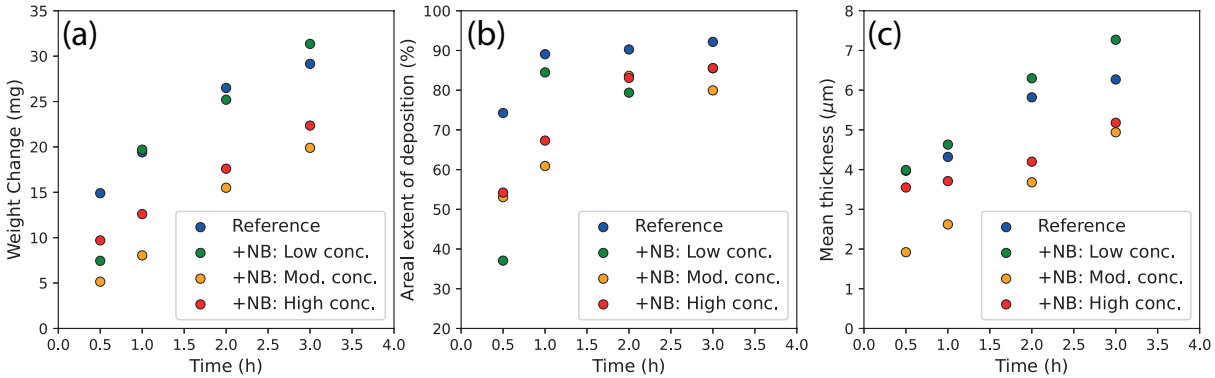

Figure 2: (a) Weight changes of the calcite deposited on the substrate surface in the 20°C solution. (b) Areal extents of the calcite covering the substrate surface in the 20°C solution. (c) Averaged thicknesses of the calcite deposited on the substrate surface in the 20°C solution. Blue points: reference solution; Green points: low number density air-nanobubbles containing solution; Orange points: moderate number density air-nanobubbles containing solution; Red points: high number density air-nanobubbles containing solution.

Surprisingly, we also found from the high-magnification (×1000) SEM images that air-nanobubbles retarded the crystal growth rate of calcite for all the studied periods 0.5–4.0 h at 20°C (Figure 3). The retardation differed with the different number densities of nanobubbles added to the solution. For example, our image analyses (see Section 2.2) using the high magnification (×1000) SEM images (Figure 3) showed that the calcite crystal sizes in the low-, moderate- and high-number density air-nanobubbles containing solution in the first 0.5 h were 2.98±1.51, 2.26±1.13, and 2.48±1.23 μm (Mean±1STD), respectively (Figure 4), yielding 59–78% of the size in the reference solution (3.84±2.20 μm). Such retardation of calcite crystal growth in the air-nanobubbles-containing solution was found even after 1.0 h, and the crystal sizes in the air-nanobubbles-containing solution after 1.0 h were 64–84 % of the size in the reference solution (4.51±2.38 μm). The level of retardation in the presence of air nanobubbles was most significant after 4.0 h, reducing the mean size in the air-nanobubbles-containing solution to 47% of that in the reference solution. The retardation was not prominent in the low-number density air-nanobubbles containing solution for 2.0, 3.0 and 4.0 h, as expected from the measured weight changes reported above. In general, however, it was slightly greater with the moderate- and high-number densities of nanobubbles (Figures 3 and 4). Interestingly, irregular-shaped calcite was often produced in the air-nanobubbles-containing solution, in contrast to rhombohedral calcite in the reference solution throughout the studied 4 hours (Figure 3).

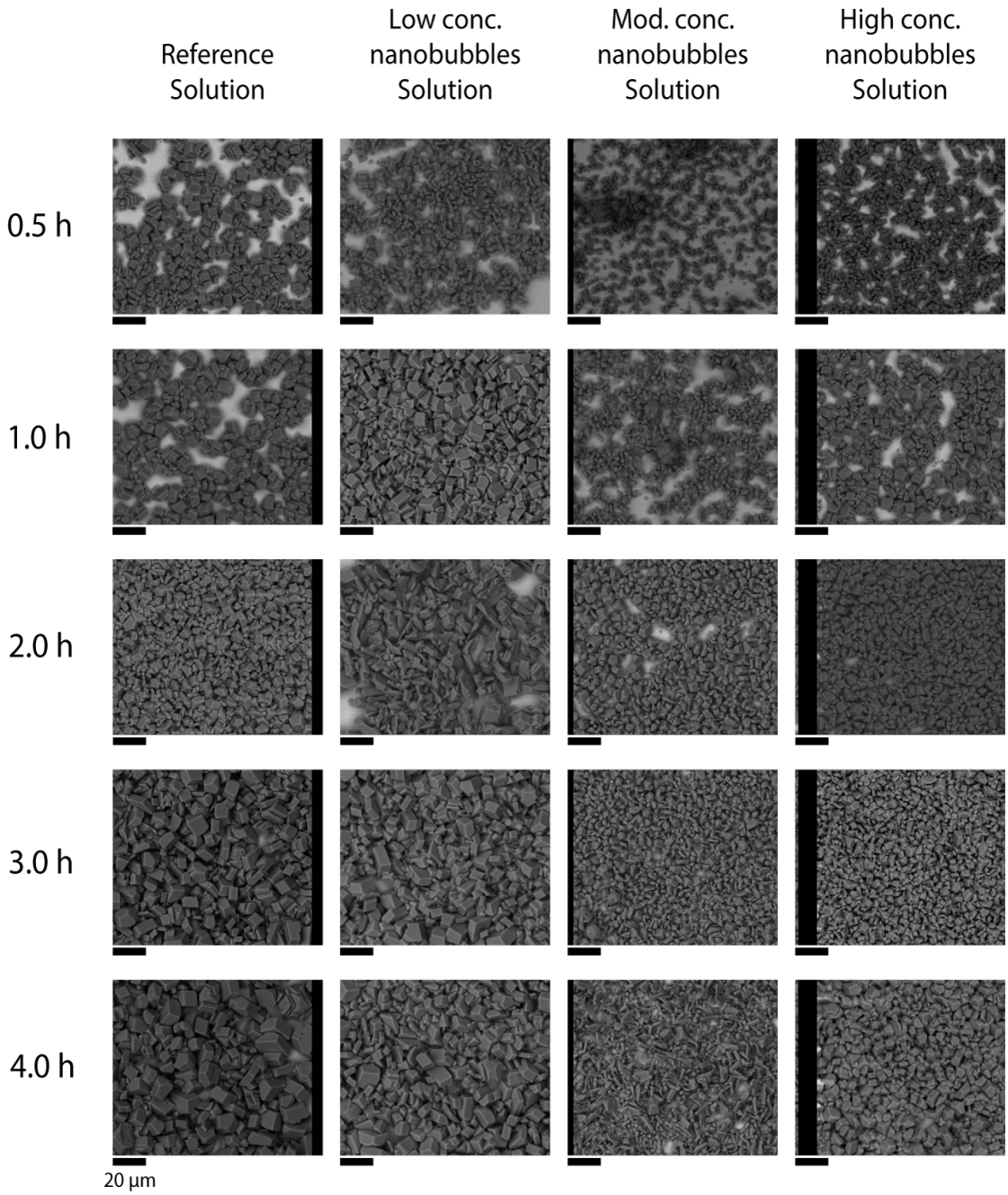

Figure 3: SEM images (×1000 magnification) of calcite crystal after 0.5, 1.0, 2.0, 3.0 and 4.0 h in the reference solution and the air-nanobubbles containing solutions with low-, moderate- and high-bubble number densities at 20°C. A black scale bar indicates 20 µm.

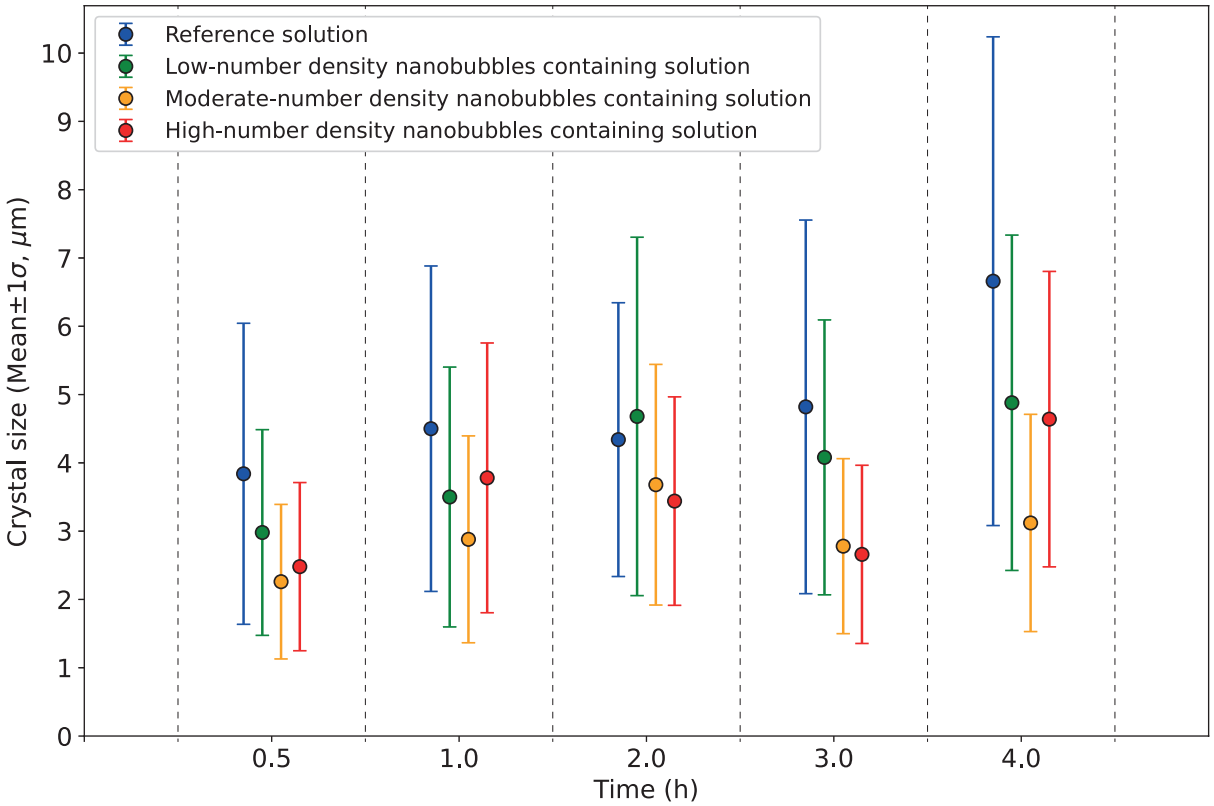

Figure 4: Changes in calcite crystal sizes (Mean±1STD μm) after 0.5, 1.0, 2.0, 3.0 and 4.0 h in the reference solution and the air-nanobubbles-containing solutions with low- to high-bubble number densities at 20°C.

3.2. Results at 88°C

To examine whether air nanobubbles in the high-temperature fluid retard the growth of calcite crystal as seen in the experiment at 20°C, we observed the crystal growth of calcium carbonate on the substrate surfaces for the first 3 hours (see Section 2.2) immersed in the reference solution and the solution containing a high-number density of air nanobubbles (continuous nanobubble generation for 30 min) kept at 88.0±0.5°C. Immersed substrates were sampled from the reference solution and the air-nanobubbles-containing solution after 0.5, 1.0, 2.0, and 3.0 h.

Amounts of the calcite deposited on the substrate surface increased gradually through time, from 13.7 mg (0.5 h) to 48.6 mg (3.0 h) for the reference solution. In the high-number density air-nanobubbles-containing solution, the weight changes were lower than those in the reference solution likewise we found in the experiment at 20°C. For example, the weight changes in the air-nanobubbles containing solution were 13.0 mg (1.0 h), 28.8 mg (2.0 h), and 39.1 mg (3.0 h), indicating that air nanobubbles helped inhibit up to 38% of calcite deposition. Also, areal extents of calcite deposition on the substrate surface in the air-nanobubbles containing solution were lower than those in the reference solution throughout the studied 3 hours. The resulting averaged thickness of calcite deposition on the substrate surfaces in the air-nanobubbles-containing solution was generally less than that in the reference solution, showing air nanobubbles inhibited up to 42% in thickness compared with the reference solution.

When looking at the high-modification SEM images of calcite crystals, we found the retardation of calcite crystal growth in the presence of air nanobubbles, as seen in the

experiment at 20°C (Figure 5). For example, the average sizes of calcite crystals in the air-nanobubbles-containing solution after 0.5 h, 1.0 h, and 3.0 h were 2.39±1.07, 2.99±1.41, and 3.09±1.23 μm, respectively, presenting 93%, 78%, 67% of those in the reference solution. The results indicate that air nanobubbles in the high-temperature fluid retard the calcite crystal growth, while that the magnitude of retardation was less than that at 20°C.

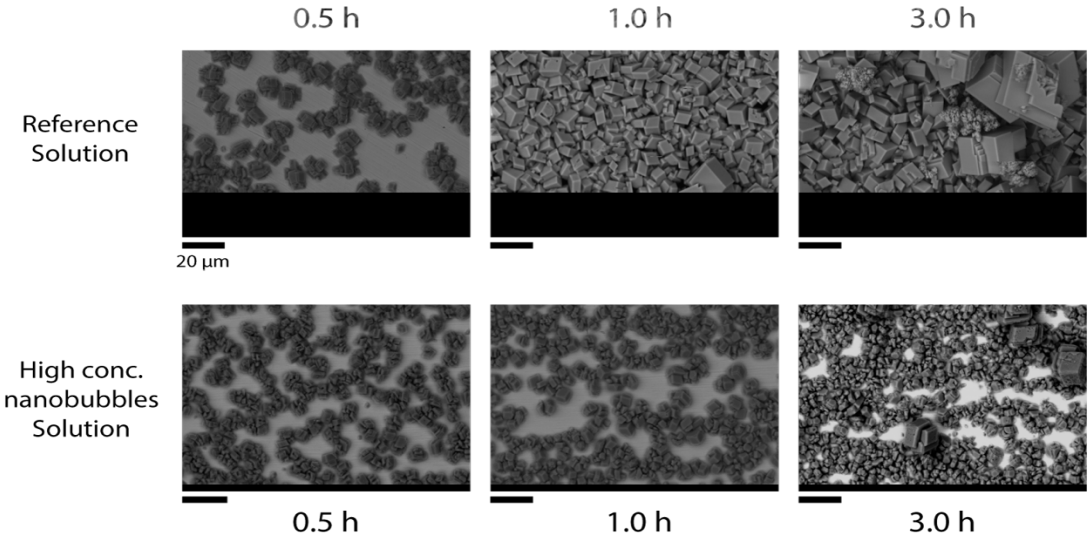

Figure 5: SEM images (×1000) and sizes (Mean±1STD μm) of calcite crystal after 0.5, 1.0, and 3.0 h in the reference and the high number density air-nanobubbles containing solutions at 88°C. A black scale bar indicates 20 μm.

3.3. Influence of nanobubbles on the calcite growth

Nanobubbles play significant roles in various physicochemical processes at the liquid-solid interfaces. Many previous studies show microbubbles and nanobubbles can involve in the micro- and nano-material fabrications. For example, Aquilano et al. [38] report the nucleation of calcite crystals at the surfaces of CO_2 microbubbles. Fan & Wang [39] suggest nanobubbles can be templates for the formation of tube-shaped vaterite crystals. In this study, we have found, for the first time to our knowledge, that air nanobubbles reduce the growth rate of calcite by up to ~50% and inhibit the calcite deposition on the steel surface at tested temperatures. Intuitively, our results suggest that the number density of nanobubbles should somehow be reduced as much as possible when we aim to avoid the reduction in the growth rate of calcite crystal, given that nanobubbles retard the crystal growth. Nanobubbles can exist both in the bulk of the liquid and on the liquid-solid interface (i.e., crystal surface and metal substrate). When most nanobubbles are present in bulk, their role in mitigating homogenous nucleation and bulk crystallization may be more dominant than inhibiting heterogeneous nucleation and surface crystallization. In contrast, when most nanobubbles are present as surface nanobubbles, they may facilitate mitigating calcite crystal growth by inhibiting heterogeneous nucleation rather than inhibiting homogenous nucleation. Below, we will discuss several possible mechanisms regarding how nanobubbles retard the calcite crystal growth and inhibit calcite deposition.

3.3.1. Solid-liquid interfacial tension on the crystal surface

Let us consider the classical nucleation theory (CNT) that represents the simplest and most widely used theory that describes a process of crystal nucleation [40,41]. The CNT theory and the Wilson-Frenkel law can be used to qualitatively understand the effect of interfacial tension upon the crystal growth, although they are based on major assumptions that allow simplifying the complex processes [41]. Using the CNT theory and the Wilson-Frenkel law, the steady-state rate of nucleation per unit time per unit volume (J) and the crystal growth rate ($\dot{R}$) can be expressed by:

$$J = J_0 \, exp\left(-\frac{16\pi\Omega^2\sigma^3}{3k_BT(\Delta\mu)^2}\right), \quad (2)$$

$$\dot{R} \sim \frac{K}{k_BT}\left(\Delta\mu - \frac{2\Omega\sigma}{R}\right), \quad (3)$$

where J_0 is the kinetic pre-factor, R is the effective radius, Ω is the volume of a molecule, σ is the interfacial tension of the interface between the nucleus and the bulk phase, k_B is Boltzmann's coefficient, T is the absolute temperature, $\Delta\mu$ is the difference in chemical potential between the liquid and the crystalline phase the nucleus is forming in minus the chemical potential of the phase nucleating, and K is the kinetic coefficient (see Appendix A). It is clear that the crystal growth rate and the nucleation rate decrease with an increase in solid-liquid interfacial tension from equations (2) and (3).

Several previous studies report that nanobubbles on the graphite substrates immersed in water can decrease their liquid-gas surface tension, while the small size of nanobubbles we studied may show a higher surface tension than that of water [42,43]. On the other hand, few works studied whether the solid-liquid interfacial tension can change in the presence of nanobubbles in the solid-liquid interface. Ohgaki et al. [16] suggested that the formation of a strong hydrogen bond network at the surface of nanobubbles can help the greater solid-liquid interfacial tension. Our results revealed that air-nanobubbles retard the crystal growth rate and the retardation is already seen in the first 30 min (Figures 3 and 4). Therefore, this retardation could be explained by the intensification of solid-liquid interfacial tension due to the presence of nanobubbles attached to the surface of nuclei of calcium carbonate (Figure 6), given that the change in the difference of chemical potential between the liquid and the crystalline phase associated with the presence of nanobubbles $\Delta\mu$ is negligible. The increase in solid-liquid interfacial tension due to nanobubbles might also help the reduction in the crystal nucleation rate of calcium carbonate, although we could not identify the effect in our experiment. These two effects of nanobubbles upon the interfacial tension of the interface between the nucleus and the bulk phase might significantly mitigate the crystal nucleation and growth of calcite. The less retardation in our experiment at the high-temperature condition as compared with that at 20°C might be explained by the fact that the interfacial tension decreases with the increase of temperature (e.g., Eötvös rule [44,45]) as well as the instability of nanobubbles adsorbed on the crystal surface.

3.3.2. Bubble mattress

Nanobubbles placed on a solid surface can exert a strong influence on the surface. Our results showed that weight changes of steel substrates are smaller with the presence of nanobubbles, and their effect was more significant with a higher number density of nanobubbles (Figure 2). In addition to their role in the interfacial tension and thermal buffer on the crystal surface, we also expect that surface nanobubbles may play a role as a

dispersant to prevent heterogeneous nucleation of calcium carbonate crystals and/or avoid the lateral growth of deposits on the steel surface. This is because nanobubbles favor staying longer on a rough surface with the help of a pining force on a rougher surface such as the studied metal surface. When nanobubbles are placed on the steel surface, they can act as a bubble mattress on the steel surface [46] in contrast to microbubbles that may just be washed away [47]. The nanobubble mattress can isolate the steel surface from the fluid for a further chemical reaction [27,48]. Also, the surface nanobubbles can simply play a role in thickening the fluid boundary layer on the steel surface [28], resulting in lengthening the path of calcium carbonate particles to the steel surface. Therefore, we would suggest that the surface nanobubbles could act as a nanoscale surface coating material by generating a bubble mattress for preventing from exposing the initiated active interface to the liquid.

Crystallization of new liquidus phases releases latent heat at the interfaces, thereby the latent heat should be conducted into the bulk for the crystal to grow [49]. When the nuclei are subject to the solution in the absence of nanobubbles, the heat conduction is simply governed by the thermal conductivity of the solution. Very few studies provided the thermal effect of nanobubbles on the liquid-solid interface relevant to this study. However, when nanobubbles are placed on the surfaces of nuclei or growth sites, the heat conduction on the liquid-solid interface is more or less hampered because they are gas entities and have much lower thermal conductivity than the liquid has, resulting in retarding the crystal growth (Figure 6). This further suggests that covering a higher concentration of nanobubbles on the surface of the nucleus or growth sites makes it more difficult to release latent heat into the bulk and grow. Therefore, our results that showed the retardation of calcite crystal growth in the presence of nanobubbles, as well as its intensification with a higher number density of nanobubbles (Figures 3 and 4), could be explained by that surface nanobubbles play a significant role in thermal buffering of the crystal surface. The generation of irregular-shaped calcite crystals in the air-nanobubbles containing solution (Figure 3) might be attributed to the fact that surface nanobubbles were not placed evenly on the crystal surface, allowing heterogeneous thermal buffering on the crystal surface.

Furthermore, the nanoscopic bubble mattress can also cover the terraces and steps of the crystalline interface. Calcite surfaces are composed of the crystallographic faces (0 0 1), (1 1 0), (0 1 2) and (1 0 4), and the overall interface properties of calcite crystal are dominated by the properties of the (1 0 4) face due to the low energy and the resulting high abundance [50 – 52]. When nanobubbles are placed on the terraces of the (1 0 4) faces, they serve as impurities and reduce the free growth sites lowering the free surface energy on the crystal interface. Here, when assuming the Davey-Mullin model in the presence of foreign species [53,54], the growth rate of the given face can simply be proportional to $(1 - \theta_{nb})$, where θ_{nb} is the fraction of crystal surface covered by nanobubbles. This can explain our results that a higher number density of nanobubbles showed greater retardation of growth rate most likely due to increasing their surface coverage of the terraces. Also, the surface nanobubbles on the terraces ahead of migrating steps might function as the step pinning and/or preferentially pinned at the obtuse and acute step edges, encouraging to inhibit the calcite crystal growth (Figure 6). The step pinning by adsorbed impurities is widely accepted to inhibit crystal growth [55 – 60], while the step height is a few Å [56] which is one or two orders of magnitude smaller than the height of surface nanobubbles [61].

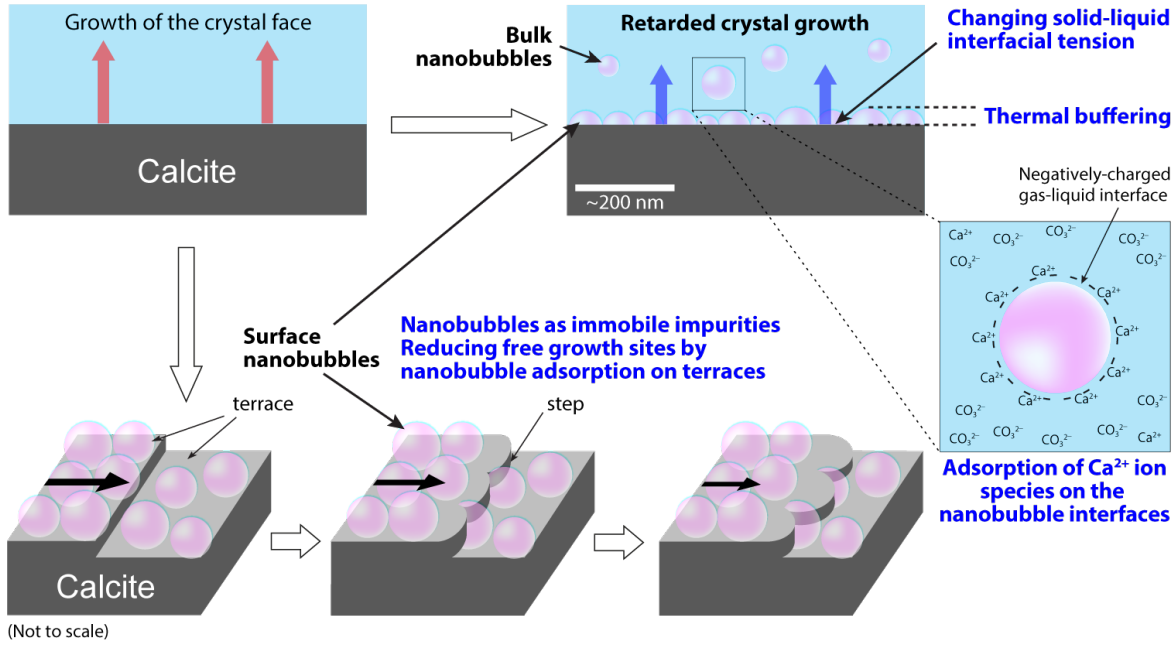

Figure 6: Possible mechanisms how nanobubbles retard the calcite crystal growth.

3.3.3. Other possible mechanisms

Other than the roles of nanobubbles discussed in the earlier sections, we also anticipate the electrochemical effect of bulk nanobubbles. For the calcite growth both Ca^{2+} and CO_3^{2-} ions need to be brought to the surface of the growth site, and thereby the Ca^{2+} to CO_3^{2-} ratio is one of the key factors determining the calcite growth rate [11,12]. Nanobubbles are negatively charged at pH > 5 [26,28,62] because of the preferential adsorption of OH^- in the first layers of water molecules at the gas-liquid interface [63]. Thus, nanobubbles are capable of the physical adsorption of Ca^{2+} ion species on the nanobubble interfaces, reducing the chance of Ca^{2+} ions combining with CO_3^{2-} ions (Figure 6). This suggests that nanobubbles can significantly decrease the Ca^{2+} to CO_3^{2-} ratio on the liquid-solid interface, which results in reducing the rates of nucleation and crystal growth of calcite.

Nanobubbles are known to withstand more than several hours and often up to several months [16 – 18]. Several of them are subject to bubble coalescence allowing them to grow, and once they are placed on the solid surface they probably contribute to thermal buffering (Section 3.3.2), generation of bubble mattress (Section 3.3.3) and flotation that result in inhibiting agglomeration and crystal growth of calcium carbonate. However, nanobubbles may swell and burst in the bulk liquid, and some of them may shrink, collide with each other or are subject to Ostwald ripening, and they eventually collapse within a couple of minutes or much shorter than the time [64]. When nanobubbles burst, they can be energetic enough to disperse their neighboring particles because of their extremely high internal pressures, as expected from the Young-Laplace equation (e.g., Ref. [15]). Furthermore, cavitation bubbles cause mechanical damage and can generate high-energy electromagnetic radiation. In this sonoluminescence, the temperature rise is reached rapidly during bubble collapse due to adiabatic compression and light is emitted. Here, an extremely high temperature can be archived with more than 10,000 kelvins within several 100's of picoseconds [65 – 67]. Such bubble collapse can only heat a tiny volume near the

bubbles to very high temperatures. Although the nucleation rate of calcium carbonate increases with temperature (equation (3)), the crystal growth rate decreases linearly with an increase in temperature as found in equation (2). Therefore, the sonoluminescence during some collapses of surface nanobubbles could encourage to retard the crystal growth of calcium carbonate through the extreme and rapid temperature rise locally on the crystal surface.

4. Conclusions

This study has paused the question of whether nanobubbles as the environmental-friendly and inexpensive additives inhibit or promote the calcite crystal growth. We found, for the first time to our knowledge, that air nanobubbles retarded the rate of calcite crystal growth by up to 50% for the first 4 hours in stational pure water at temperatures of 20°C and 88°C. The retardation could differ with the different number densities of air nanobubbles added to the solution at the temperature of 20°C. A higher number density of air nanobubbles generally showed slightly higher retardation. We suggest that bulk and surface air nanobubbles can influence the crystal growth either through changing solid-liquid interfacial tension on the crystal surface, reducing the free growth areas due to adsorption of nanobubbles at calcite terraces, playing roles in bubble mattress and thermal buffering on the crystal surface, reducing the chance of Ca^{2+} to combine with CO_3^{2-} by the adsorption of Ca^{2+} on the nanobubble interface, or combinations of them; however, more definitive investigations are necessary for clarifying which factors are a primary one or whether combinations of different effects change the magnitude of retardation. Also, it remains to open to understanding whether the effectiveness of nanobubbles on the crystal growth retardation differs with the choice of gases (e.g., N_2, O_2, CO_2, and air) for generating nanobubbles, typical diameters of nanobubbles, pH conditions, and under dynamic conditions instead of static conditions we studied, which should be studied in future works. Anyhow, our finding highlights that air nanobubbles can be used as an effective “green” inhibitor for the crystal growth of calcium carbonate in broad industrial areas at least under certain conditions.

Declaration of Competing Interest

The authors declare that they have no known competing financial interests or personal relationships that could have appeared to influence the work reported in this paper.

Acknowledgments

The authors are grateful to T. Yokoyama, A. Aikawa, K. Sasaki, Y. Sugai, N. Okibe, Y. Kiyota, T. Kodama, and S. Jalilinasrabady for discussion and their comments to our earlier study. The authors also thank the reviewers for their helpful comments. This work was supported by the Frontiers in Engineering Research from Kyushu University (FY2020-2021) and JSPS KAKENHI Grant-in-Aid for Early-Career Scientists (JP21K14576).

Appendix A. The rates of crystal nucleation and crystal growth

In the CNT theory, density fluctuations in a metastable phase cause the formation of clusters of prenucleation. They assemble and disassemble continuously until attaining a certain critical size, and once reaching the certain critical size they become stable and grow spontaneously to form crystal nuclei. The thermodynamic description of this process can be defined by the total free-energy change required for cluster formation (ΔG) as a sum of the free energy change for the phase transformation (ΔG_v) and the free energy change for the formation of a surface (ΔG_s), so that:

$$\Delta G = \Delta G_v + \Delta G_s = \alpha L^3 \Delta G_v + \beta L^2 \sigma, \quad \text{(A.1)}$$

where σ is the interfacial tension of the interface between the nucleus and the bulk phase, and α and β are the volume and area shape factors for the characteristic length L, respectively. Assuming spherical clusters, equation (A.1) can be rewritten as:

$$\Delta G = -\frac{4\pi R^3}{3\Omega}\Delta\mu + 4\pi R^2 \sigma, \quad \text{(A.2)}$$

where R is the effective radius, Δμ is the difference in chemical potential between the liquid and the crystalline phase the nucleus is forming in minus the chemical potential of the phase nucleating (i.e., the solid state is more stable than the liquid, decreasing the Gibbs free energy of the system), and Ω is the volume of a molecule [68]. Then we have the infinitesimal change of free energy $\delta(\Delta G)$ with an infinitesimal radius increase δR from equation (A.2):

$$\delta(\Delta G) = \left(-\frac{4\pi R^2}{\Omega}\Delta\mu + 8\pi R\sigma\right)\delta R. \quad \text{(A.3)}$$

Here, as number of molecules of crystal $\delta N = (4\pi R^2 \delta R)/\Omega$ increases, the infinitesimal change of free energy per one molecule is expressed from equation (A.3):

$$\frac{\delta(\Delta G)}{\delta N} = -\left(\Delta\mu - \frac{2\Omega\sigma}{R}\right), \quad \text{(A.4)}$$

which indicates that the driving force for crystal growth is reduced by $2\Omega\sigma/R$ from the chemical potential Δμ.

Given that the total crystal growth rate $\dot{R}$ represents the difference between the rate of deposition in crystal and the rate of evaporation from crystal at time, the simple Wilson-Frenkel law for the growth rate in the absence of the effect of interfacial tension is expressed by:

$$\dot{R} = K\left(exp\left(\frac{\Delta\mu}{k_B T}\right) - 1\right), \quad \text{(A.5)}$$

where K is the kinetic coefficient, k_B is Boltzmann's coefficient and T is the absolute temperature [69]. Therefore, when taking into account the effect of interfacial tension, the crystal growth rate for small enough Δμ can be approximated from equations (A.4) and (A.5):

$$\dot{R} \sim \frac{K}{k_B T}\left(\Delta\mu - \frac{2\Omega\sigma}{R}\right), \quad \text{(A.6)}$$

which indicates that the crystal growth rate decreases linearly with an increase in interfacial tension σ. The free energy reaches its maximum at a value of the critical size R_c. For clusters larger than the critical size, the total free energy decreases, and thus growth becomes energetically favorable. The critical size can be easily found by setting the derivative of ΔG to zero, $\delta(\Delta G)/\delta R = 0$ in equation (A.2), i.e., $R_c = 2\Omega\sigma/\Delta\mu$. Thus, the maximum value of the free energy change "activation barrier for nucleation" ΔG_c [40,54] is obtained from equation (A.2):

$$\Delta G_c = \frac{16\pi}{3}\frac{\Omega^2\sigma^3}{(\Delta\mu)^2}. \quad \text{(A.7)}$$

Therefore, the steady-state rate of nucleation J per unit time per unit volume (the von Weimarn rules nucleation rate [70]) is expressed in the Arrhenius form by substituting equation (A.7):

$$J = J_0\ exp\left(-\frac{\Delta G_c}{k_B T}\right) = J_0\ exp\left(-\frac{16\pi\Omega^2\sigma^3}{3k_B T(\Delta\mu)^2}\right), \quad \text{(A.8)}$$

where J_0 is the kinetic pre-factor [54,71]. Equation (A.8) indicates that the nucleation rate J increases with temperature T and decreases with an increase in interfacial tension σ.

References

[1] J.J. De Yoreo, P.U.P.A. Gilbert, N.A.J.M. Sommerdijk, R.L. Penn, S. Whitelam, D. Joester, H. Zhang, J.D. Rimer, A. Navrotsky, J.F. Banfield, A.F. Wallace, F.M. Michel, F.C. Meldrum, H. Colfen, P.M. Dove, Crystallization by particle attachment in synthetic, biogenic, and geologic environments, Science 349 (2015) aaa6760. https://doi.org/10.1126/science.aaa6760

[2] F.C. Meldrum, C. O'Shaughnessy, Crystallization in Confinement, Adv. Mater. 32 (2020) 2001068. https://doi.org/10.1002/adma.202001068

[3] A.-W. Xu, Y. Ma, H. Cölfen, Biomimetic mineralization, J. Mater. Chem. 17 (2007) 415–449. https://doi.org/10.1039/B611918M

[4] L. Lindfors, S. Forssén, J. Westergren, U. Olsson, Nucleation and crystal growth in supersaturated solutions of a model drug, J. Colloid Interface Sci. 325 (2008) 404–413. https://doi.org/10.1016/j.jcis.2008.05.034

[5] F. Jones, M.I. Ogden, Controlling crystal growth with modifiers, CrystEngComm 12 (2010) 1016–1023. https://doi.org/10.1039/B918849E

[6] P. Falkowski, R.J. Scholes, E. Boyle, J. Canadell, D. Canfield, J. Elser, N. Gruber, K. Hibbard, P. Högberg, S. Linder, F.T. Mackenzie, B. Moore III, T. Pedersen, Y. Rosenthal, S. Seitzinger, V. Smetacek, W. Steffen, The Global Carbon Cycle: A Test of Our Knowledge of Earth as a System, Science 290 (2000) 291–296. https://doi.org/10.1126/science.290.5490.291

[7] J.N. Bracco, A.G. Stack, C.I. Steefel, Upscaling Calcite Growth Rates from the Mesoscale to the Macroscale, Environ. Sci. Technol. 47 (2013) 7555–7562. https://doi.org/10.1021/es400687r

[8] T. Ogino, T. Suzuki, K. Sawada, The formation and transformation mechanism of calcium carbonate in water, Geochim. Cosmochim. Acta 51 (1987) 2757–2767. https://doi.org/10.1016/0016-7037(87)90155-4

[9] D. Gebauer, A. Völkel, H. Cölfen, Stable Prenucleation Calcium Carbonate Clusters, Science 322 (2008) 1819–1822. https://doi.org/10.1126/science.1164271

[10] J.D. Rodriguez-Blanco, S. Shaw, L.G. Benning, The kinetics and mechanisms of amorphous calcium carbonate (ACC) crystallization to calcite, via vaterite., Nanoscale 3 (2011) 265–271. https://doi.org/10.1039/C0NR00589D

[11] J.N. Bracco, M.C. Grantham, A.G. Stack, Calcite Growth Rates As a Function of Aqueous Calcium-to-Carbonate Ratio, Saturation Index, and Inhibitor Concentration: Insight into the Mechanism of Reaction and Poisoning by Strontium, Cryst. Growth Des. 12 (2012) 3540–3548. https://doi.org/10.1021/cg300350k

[12] M.P. Andersson, S. Dobberschütz, K.K. Sand, D.J. Tobler, J.J. De Yoreo, S.L.S. Stipp, A Microkinetic Model of Calcite Step Growth, Angew. Chem. Int. Ed. 55 (2016) 11086–11090. https://doi.org/10.1002/anie.201604357

[13] M.R. Nielsen, K.K. Sand, J.D. Rodriguez-Blanco, N. Bovet, J. Generosi, K.N. Dalby, S.L.S. Stipp, Inhibition of Calcite Growth: Combined Effects of Mg^{2+} and SO_4^{2-}, Cryst. Growth Des. 16 (2016) 6199–6207. https://doi.org/10.1021/acs.cgd.6b00536

[14] S. Dobberschütz, M.R. Nielsen, K.K. Sand, R. Civioc, N. Bovet, S.L.S. Stipp, M.P. Andersson, The mechanisms of crystal growth inhibition by organic and inorganic inhibitors, Nat. Commun. 9 (2018) 1578. https://doi.org/10.1038/s41467-018-04022-0

[15] D. Lohse, X. Zhang, Surface nanobubbles and nanodroplets, Rev. Mod. Phys. 87 (2015) 981–1035. https://doi.org/10.1103/RevModPhys.87.981

[16] K. Ohgaki, N.Q. Khanh, Y. Joden, A. Tsuji, T. Nakagawa, Physicochemical approach to nanobubble solutions, Chem. Eng. Sci. 65 (2010) 1296–1300. https://doi.org/10.1016/j.ces.2009.10.003
[17] R. Etchepare, H. Oliveira, M. Nicknig, A. Azevedo, J. Rubio, Nanobubbles: Generation using a multiphase pump, properties and features in flotation, Miner. Eng. 112 (2017) 19–26. https://doi.org/10.1016/j.mineng.2017.06.020
[18] E.D. Michailidi, G. Bomis, A. Varoutoglou, G.Z. Kyzas, G. Mitrikas, A.C. Mitropoulos, E.K. Efthimiadou, E.P. Favvas, Bulk nanobubbles: Production and investigation of their formation/stability mechanism, J. Colloid Interface Sci. 564 (2020) 371–380. https://doi.org/10.1016/j.jcis.2019.12.093
[19] J.R.T. Seddon, D. Lohse, W.A. Ducker, V.S.J. Craig, A Deliberation on Nanobubbles at Surfaces and in Bulk, ChemPhysChem 13 (2012) 2179–2187. https://doi.org/10.1002/cphc.201100900
[20] M. Nakagawa, A. Kioka, K. Tagomori, Nanobubbles as friction modifier, Tribol. Int. 165 (2022) 107333. https://doi.org/10.1016/j.triboint.2021.107333
[21] H. Teshima, H. Kusudo, C. Bistafa, Y. Yamaguchi, Quantifying interfacial tensions of surface nanobubbles: How far can Young's equation explain?, Nanoscale 14 (2022) 2446–2455. https://doi.org/10.1039/D1NR07428H
[22] X. Zhang, H. Lhuissier, C. Sun, D. Lohse, Surface Nanobubbles Nucleate Microdroplets, Phys. Rev. Lett. 112 (2014) 144503. https://doi.org/10.1103/PhysRevLett.112.144503
[23] M. Li, X. Ma, J. Eisener, P. Pfeiffer, C.-D. Ohl, C. Sun, How bulk nanobubbles are stable over a wide range of temperatures, J. Colloid Interface Sci. 596 (2021) 184–198. https://doi.org/10.1016/j.jcis.2021.03.064
[24] X.H. Zhang, N. Maeda, V.S.J. Craig, Physical Properties of Nanobubbles on Hydrophobic Surfaces in Water and Aqueous Solutions, Langmuir 22 (2006) 5025–5035. https://doi.org/10.1021/la0601814
[25] G. Liu, V.S.J. Craig, Improved Cleaning of Hydrophilic Protein-Coated Surfaces using the Combination of Nanobubbles and SDS, ACS Appl. Mater. Interfaces 1 (2009) 481–487. https://doi.org/10.1021/am800150p
[26] J. Zhu, H. An, M. Alheshibri, L. Liu, P.M.J. Terpstra, G. Liu, V.S.J. Craig, Cleaning with Bulk Nanobubbles, Langmuir 32 (2016) 11203–11211. https://doi.org/10.1021/acs.langmuir.6b01004
[27] A. Aikawa, A. Kioka, M. Nakagawa, S. Anzai, Nanobubbles as corrosion inhibitor in acidic geothermal fluid, Geothermics 89 (2021) 101962. https://doi.org/10.1016/j.geothermics.2020.101962
[28] A. Kioka, M. Nakagawa, Theoretical and experimental perspectives in utilizing nanobubbles as inhibitors of corrosion and scale in geothermal power plant, Renew. Sustain. Energy Rev. 149 (2021) 111373. https://doi.org/10.1016/j.rser.2021.111373
[29] Y.-Y. Kim, C.L. Freeman, X. Gong, M.A. Levenstein, Y. Wang, A. Kulak, C. Anduix-Canto, P.A. Lee, S. Li, L. Chen, H.K. Christenson, F.C. Meldrum, The Effect of Additives on the Early Stages of Growth of Calcite Single Crystals, Angew. Chem. Int. Ed. 56 (2017) 11885–11890. https://doi.org/10.1002/anie.201706800
[30] A.K.A. Ahmed, C. Sun, L. Hua, Z. Zhang, Y. Zhang, W. Zhang, T. Marhaba, Generation of nanobubbles by ceramic membrane filters: The dependence of bubble size and zeta potential on surface coating, pore size and injected gas pressure, Chemosphere 203 (2018) 327–335. https://doi.org/10.1016/j.chemosphere.2018.03.157

[31] D.L. Parkhurst, C.A.J. Appelo, Description of input and examples for PHREEQC version 3: a computer program for speciation, batch-reaction, one-dimensional transport, and inverse geochemical calculations (No. 6-A43), US Geological Survey (2013). https://doi.org/10.3133/tm6A43
[32] L.N. Plummer, T.M.L. Wigley, D.L. Parkhurst, The kinetics of calcite dissolution in CO2-water systems at 5 degrees to 60 degrees C and 0.0 to 1.0 atm CO2, Am. J. Sci. 278 (1978) 179–216. https://doi.org/10.2475/ajs.278.2.179
[33] A. Rabbani, S. Salehi, Dynamic modeling of the formation damage and mud cake deposition using filtration theories coupled with SEM image processing, J. Nat. Gas Sci. Eng. 42 (2017) 157–168. https://doi.org/10.1016/j.jngse.2017.02.047
[34] N. Otsu, A Threshold Selection Method from Gray-Level Histograms, IEEE Trans. Syst. Man. Cybern. 9 (1979) 62–66. https://doi.org/10.1109/TSMC.1979.4310076
[35] T.W. Ridler, S. Calvard, Picture Thresholding Using an Iterative Selection Method, IEEE Trans. Syst. Man. Cybern. 8 (1978) 630–632. https://doi.org/10.1109/TSMC.1978.4310039
[36] J. Schindelin, I. Arganda-Carreras, E. Frise, V. Kaynig, M. Longair, T. Pietzsch, S. Preibisch, C. Rueden, S. Saalfeld, B. Schmid, J.-Y. Tinevez, D.J. White, V. Hartenstein, K. Eliceiri, P. Tomancak, A. Cardona, Fiji: an open-source platform for biological-image analysis, Nat. Methods 9 (2012) 676–682. https://doi.org/10.1038/nmeth.2019
[37] C.A. Schneider, W.S. Rasband, K.W. Eliceiri, NIH Image to ImageJ: 25 years of image analysis, Nat. Methods 9 (2012) 671–675. https://doi.org/10.1038/nmeth.2089
[38] D. Aquilano, E. Costa, A. Genovese, F. Roberto Massaro, L. Pastero, M. Rubbo, Hollow rhombohedral calcite crystals encompassing CO2 microcavities nucleated in solution, J. Cryst. Growth 247 (2003) 516–522. https://doi.org/10.1016/S0022-0248(02)01986-3
[39] Y.W. Fan, R.Z. Wang, Submicrometer-Sized Vaterite Tubes Formed Through Nanobubble-Templated Crystal Growth, Adv. Mater. 17 (2005) 2384–2388. https://doi.org/10.1002/adma.200500755
[40] R.P. Sear, Nucleation: theory and applications to protein solutions and colloidal suspensions, J. Phys. Condens. Matter 19 (2007) 033101. https://doi.org/10.1088/0953-8984/19/3/033101
[41] D. Erdemir, A.Y. Lee, A.S. Myerson, Crystal Nucleation, in: Handb. Ind. Cryst., Cambridge University Press, 2019: pp. 76–114. https://doi.org/10.1017/9781139026949.003
[42] B. Zhao, Y. Song, S. Wang, B. Dai, L. Zhang, Y. Dong, J. Lü, J. Hu, Mechanical mapping of nanobubbles by PeakForce atomic force microscopy, Soft Matter 9 (2013) 8837. https://doi.org/10.1039/c3sm50942g
[43] B. Zhao, X. Wang, Y. Song, J. Hu, J. Lü, X. Zhou, R. Tai, X. Zhang, L. Zhang, Stiffness and evolution of interfacial micropancakes revealed by AFM quantitative nanomechanical imaging, Phys. Chem. Chem. Phys. 17 (2015) 13598–13605. https://doi.org/10.1039/C5CP01366F
[44] N. K. Adam, Physics and Chemistry of Surfaces, London: Oxford University Press (1930).
[45] S.R. Palit, Thermodynamic Interpretation of the Eötvös Constant, Nature 177 (1956) 1180–1180. https://doi.org/10.1038/1771180a0
[46] J. Hyväluoma, C. Kunert, J. Harting, Simulations of slip flow on nanobubble-laden surfaces, J. Phys. Condens. Matter 23 (2011) 184106. https://doi.org/10.1088/0953-8984/23/18/184106

[47] A. Steinberger, C. Cottin-Bizonne, P. Kleimann, E. Charlaix, High friction on a bubble mattress, Nat. Mater. 6 (2007) 665–668. https://doi.org/10.1038/nmat1962
[48] M. Alheshibri, A. Al Baroot, L. Shui, M. Zhang, Nanobubbles and nanoparticles, Curr. Opin. Colloid Interface Sci. 55 (2021) 101470. https://doi.org/10.1016/j.cocis.2021.101470
[49] J.S. Langer, Instabilities and pattern formation in crystal growth, Rev. Mod. Phys. 52 (1980) 1–28. https://doi.org/10.1103/RevModPhys.52.1
[50] J. Paquette, R.J. Reeder, Relationship between surface structure, growth mechanism, and trace element incorporation in calcite, Geochim. Cosmochim. Acta 59 (1995) 735–749. https://doi.org/10.1016/0016-7037(95)00004-J
[51] F. Heberling, T.P. Trainor, J. Lützenkirchen, P. Eng, M.A. Denecke, D. Bosbach, Structure and reactivity of the calcite–water interface, J. Colloid Interface Sci. 354 (2011) 843–857. https://doi.org/10.1016/j.jcis.2010.10.047
[52] M. Bruno, F.R. Massaro, L. Pastero, E. Costa, M. Rubbo, M. Prencipe, D. Aquilano, New Estimates of the Free Energy of Calcite/Water Interfaces for Evaluating the Equilibrium Shape and Nucleation Mechanisms, Cryst. Growth Des. 13 (2013) 1170–1179. https://doi.org/10.1021/cg3015817
[53] R.J. Davey, J.W. Mullin, Growth of the {100} faces of ammonium dihydrogen phosphate crystals in the presence of ionic species, J. Cryst. Growth 26 (1974) 45–51. https://doi.org/10.1016/0022-0248(74)90197-3
[54] K. Sangwal, Additives and Crystallization Processes, John Wiley & Sons, Ltd, Chichester, UK, 2007. https://doi.org/10.1002/9780470517833
[55] K. Sangwal, Effects of impurities on crystal growth processes, Prog. Cryst. Growth Charact. Mater. 32 (1996) 3–43. https://doi.org/10.1016/0960-8974(96)00008-3
[56] K.J. Davis, P.M. Dove, J.J. De Yoreo, The Role of Mg^{2+} as an Impurity in Calcite Growth, Science 290 (2000) 1134–1137. https://doi.org/10.1126/science.290.5494.1134
[57] E. Loste, R.M. Wilson, R. Seshadri, F.C. Meldrum, The role of magnesium in stabilising amorphous calcium carbonate and controlling calcite morphologies, J. Cryst. Growth 254 (2003) 206–218. https://doi.org/10.1016/S0022-0248(03)01153-9
[58] L.E. Wasylenki, P.M. Dove, D.S. Wilson, J.J. De Yoreo, Nanoscale effects of strontium on calcite growth: An in situ AFM study in the absence of vital effects, Geochim. Cosmochim. Acta 69 (2005) 3017–3027. https://doi.org/10.1016/j.gca.2004.12.019
[59] H. Miura, Phase-Field Modeling of Step Dynamics on Growing Crystal Surface: Step Pinning Induced by Impurities, Cryst. Growth Des. 15 (2015) 4142–4148. https://doi.org/10.1021/acs.cgd.5b00762
[60] J.P. Lee-Thorp, A.G. Shtukenberg, R. V. Kohn, Effect of Step Anisotropy on Crystal Growth Inhibition by Immobile Impurity Stoppers, Cryst. Growth Des. 17 (2017) 5474–5487. https://doi.org/10.1021/acs.cgd.7b01006
[61] W. Walczyk, H. Schönherr, Dimensions and the Profile of Surface Nanobubbles: Tip–Nanobubble Interactions and Nanobubble Deformation in Atomic Force Microscopy, Langmuir 30 (2014) 11955–11965. https://doi.org/10.1021/la502918u
[62] A.J. Atkinson, O.G. Apul, O. Schneider, S. Garcia-Segura, P. Westerhoff, Nanobubble Technologies Offer Opportunities To Improve Water Treatment, Acc. Chem. Res. 52 (2019) 1196–1205. https://doi.org/10.1021/acs.accounts.8b00606
[63] J.K. Beattie, A.M. Djerdjev, G.G. Warr, The surface of neat water is basic, Faraday Discuss. 141 (2009) 31–39. https://doi.org/10.1039/B805266B

[64] T. Temesgen, T.T. Bui, M. Han, T. Kim, H. Park, Micro and nanobubble technologies as a new horizon for water-treatment techniques: A review, Adv. Colloid Interface Sci. 246 (2017) 40–51. https://doi.org/10.1016/j.cis.2017.06.011
[65] W.C. Moss, D.B. Clarke, J.W. White, D.A. Young, Hydrodynamic simulations of bubble collapse and picosecond sonoluminescence, Phys. Fluids 6 (1994) 2979–2985. https://doi.org/10.1063/1.868124
[66] S.J. Putterman, K.R. Weninger, Sonoluminescence: How Bubbles Turn Sound into Light, Annu. Rev. Fluid Mech. 32 (2000) 445–476. https://doi.org/10.1146/annurev.fluid.32.1.445
[67] M.P. Brenner, S. Hilgenfeldt, D. Lohse, Single-bubble sonoluminescence, Rev. Mod. Phys. 74 (2002) 425–484. https://doi.org/10.1103/RevModPhys.74.425
[68] F. Spaepen, Homogeneous Nucleation and the Temperature Dependence of the Crystal-Melt Interfacial Tension, Solid State Phys. 47 (1994) 1–32. https://doi.org/10.1016/S0081-1947(08)60638-4
[69] J.D. Weeks, G.H. Gilmer, Dynamics of Crystal Growth, in: I. Prigogine, S.A. Rice (Eds.), Adv. Chem. Phys., 1979: pp. 157–228. https://doi.org/10.1002/9780470142592.ch4
[70] P.P. von Weimarn, The Precipitation Laws., Chem. Rev. 2 (1925) 217–242. https://doi.org/10.1021/cr60006a002
[71] J.J. De Yoreo, P.G. Vekilov, Principles of Crystal Nucleation and Growth, Rev. Mineral. Geochem. 54 (2003) 57–93. https://doi.org/10.2113/0540057